PERGAMON

Journal of Structural Geology 23 (2001) 1299–1317

JOURNAL OF STRUCTURAL GEOLOGY

www.elsevier.nl/locate/jstrugeo

Magnetic fabrics reveal Upper Mantle Flow fabrics in the Troodos Ophiolite Complex, Cyprus

Graham J. Borradaile*, France Lagroix

Geology Department, Lakehead University, Thunder Bay, Canada P7B 5E1

Received 10 January 2000; accepted 21 November 2000

Abstract

The foliations and lineations recognized in outcrops of the Troodos mantle-sequence provide relatively few and imprecise observations of the mineral fabric. Thus, their kinematic interpretation, and any inferences about the metamorphic flow patterns are tenuous. However, every outcrop yields the anisotropy of magnetic susceptibility (AMS) from which we may infer the combined orientation–distribution response of silicates (pyroxene, serpentine) and magnetite. Furthermore, in many outcrops, the anisotropy of anhysteretic remanence (AARM) isolates the contribution of magnetite to the orientation–distribution. AMS and AARM each provide a magnitude ellipsoid whose principal directions define the orientation–distribution of several hundred minerals in each sample, and thus their flow fabric.

Within the Troodos mantle-sequence, high-temperature, semi-cataclastic silicate flow directions were uniform through volumes of $\sim$1 km^3 but differ between adjacent subareas. This reflects the scale of the heterogeneity of solid-state flow. However, averaged over the entire area of $\sim$100 km^2, the global orientation–distribution of silicate alignments were consistent, indicating early, silicate flow up to the west, away from a spreading axis that lay east of the Troodos range. On the same regional scale, later magnetite alignments indicate flow up to the north-west. The non-horizontal and non-coaxial flow stages suggest that the mantle sequence was affected by diapiric rise in the solid-state, radiating from centres which may originally have been magma chambers. The one responsible for the recorded flow patterns may have been approximately 30 km in diameter and located SE of Mount Troodos.

Keywords: Magnetic-fabric; AMS; AARM; Ophiolite; Cyprus

1. Introduction

The Troodos Complex of Cyprus is the best exposed and most well-documented example of an ophiolite sequence (Moores et al., 1984; Robinson and Malpas, 1987; Murton, 1990; Robertson, 1990). Located in the uplifted central portion of Cyprus, it provides a continuous section from Upper Mantle harzburgites, lhertzolites and dunites, through a diabase sheeted-dike complex to a pillow basalt sequence and an overlying pelagic chalk sequence (Fig. 1). The sequence suffered mild deformation during its uplift, that is attributed in part to north–south crustal compression and in part to 15% dilation by serpentinization (e.g. Gass, 1990). The Troodos Complex is in a serendipitous location, being located very close to the ancient ocean-floor spreading axis. That axis, originally east–west, now north–south, left its impression as a series of ephemeral graben, probably migrating with time from the Solea, to Mitsero and then to the Larnaca Graben progressively, all to the east of Mount Troodos (Fig. 1c). These should be regarded as local spreading axes rather than an entire mid-ocean ridge. Moreover, the Troodos region exposes a major fossil transform fracture zone, the 10-km-wide, Southern Troodos Transform Zone (SSTZ), defined on its northern margin by the Arakapas Fault (Allerton and Vine, 1987, 1991; Gass 1990). Whereas the Mount Troodos Ophiolite uplift was achieved by regional compression and serpentinization, within the SSTZ the mantle sequence rocks were elevated by extensional relay faults (op.cit.), (Fig. 1). The rocks of Cyprus, in their present position, have been rotated 90° anticlockwise, so that the fossil spreading axes presently trend north–south. Originally, however, their orientation was east–west, and below, geographic coordinates refer to the subduction in the original geographic arrangement. The entire region was located in a supra-subduction setting with northwards subduction of oceanic lithosphere beneath Troodos.

The closure of the Neo-Tethys commenced during Mid-Cretaceous ($\sim$119 Ma) with a northward subduction of the ocean floor under the region that subsequently became Cyprus. The subduction hinge stepped backwards to the

* Corresponding author. Tel.: +1-807-343-8461; fax: +1-807-346-7853.
E-mail address: borradaile@lakeheadu.ca (G.J. Borradaile).

0191-8141/01/$ - see front matter
PII: S0191-8141(00)00186-3

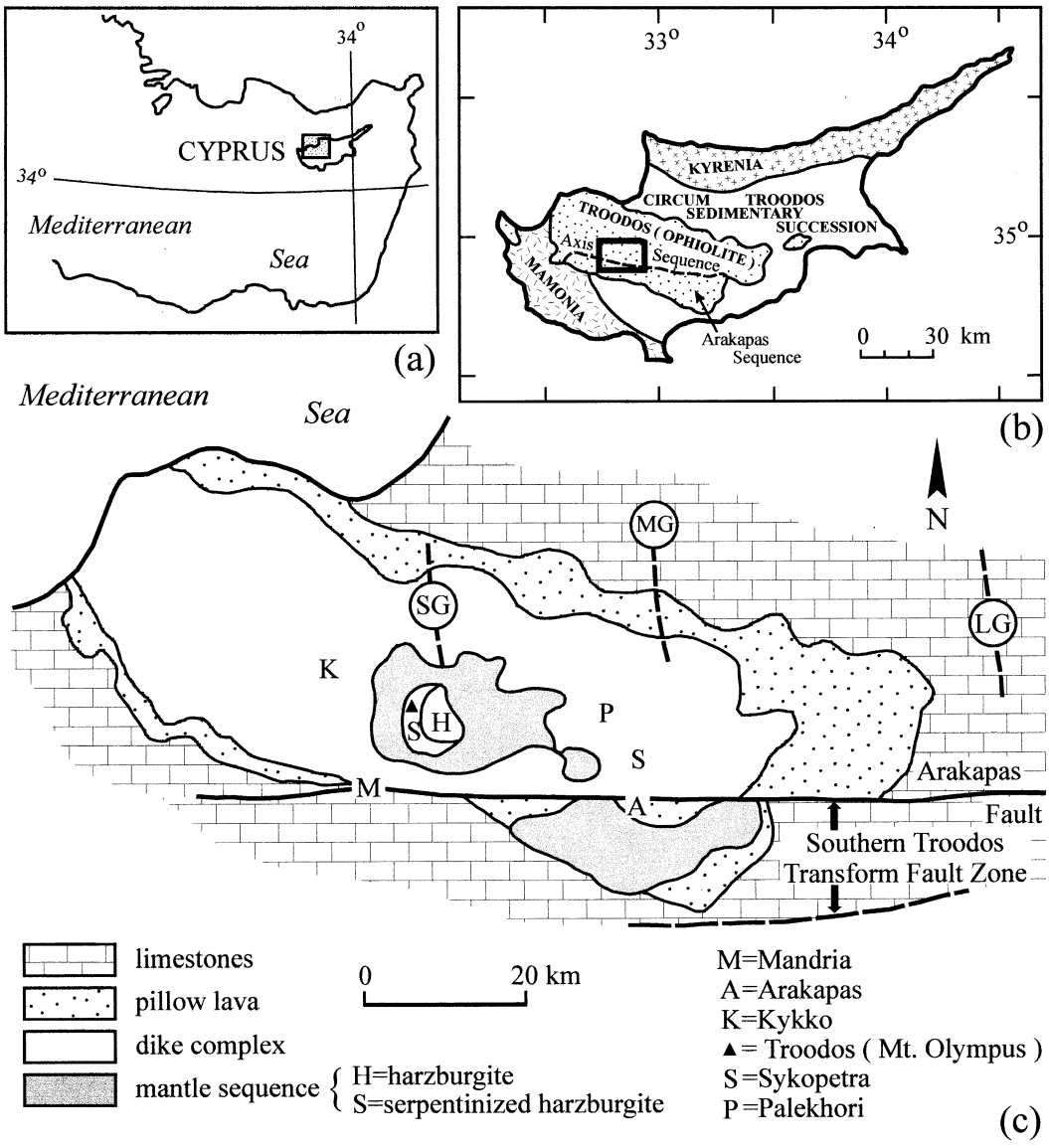

Fig. 1. The principal geological terrains of Cyprus showing the centrally uplifted Troodos Ophiolite Complex (inset above left). The main map shows that the domed Troodos Ophiolite Complex of Cyprus comprises a sequence from pelagic limestones, down through pillow lavas, sheeted dikes to upper asthenosphere harzburgites. Doming is due to regional compression and dilational-uplift due to serpentinization. Successive local sea-floor spreading axes are recognized in order as the Solea (SG), Mitsero (MG) and Larnaca Grabens (LG). Thus, the spreading direction was east–west in present-day coordinates. To the south of Mount Troodos an EW transform fault zone corroborates that spreading direction. Prior to the 90° anticlockwise rotation of the rocks of Cyprus, the original spreading direction was, of course, north–south.

south, leaving the location of Cyprus, and its Mid- to Late-Cretaceous Ophiolite sequence above the Benioff Zone. The ophiolites were then progressively rotated anticlockwise as the cover accumulated from the Late Cretaceous Troodos pillow lava sequence (~90 Ma) to the end-Cretaceous uppermost Lefkara Chalks (~65 Ma). The total anticlockwise rotation to the present day has been 90° (Clube and Robertson, 1986); thus, the spreading axes traced by the N–S rifts (Fig. 1c) were originally E–W. The mantle-sequence rocks beneath the diabase dike complex are composed of harzburgites, lhertzolites and dunites.

Recent work on exposed ophiolites suggests that the mineral flow fabrics within the mantle near oceanic spreading axes are not everywhere perpendicular to the axis (Cueleneer et al., 1988; Gass et al., 1994, pp. 16–17). Instead, the flow seems to radiate away from centres that are associated with the rise and emplacement of magma chambers. The latter may occupy volumes perhaps 10–30 km in length parallel to the spreading axis and 5–15 km in width perpendicular to the spreading axis (Fig. 2). Consequently, mineral flow fabrics diverge from the diapiric center with an overall tendency to be orthogonal to the local ridge axis. The nature of the diapiric flow is of some interest to us but in the field it is difficult to document because of the low shape-anisotropy of olivine, pyroxenes, magnetite and chromite that constitute the bulk of the

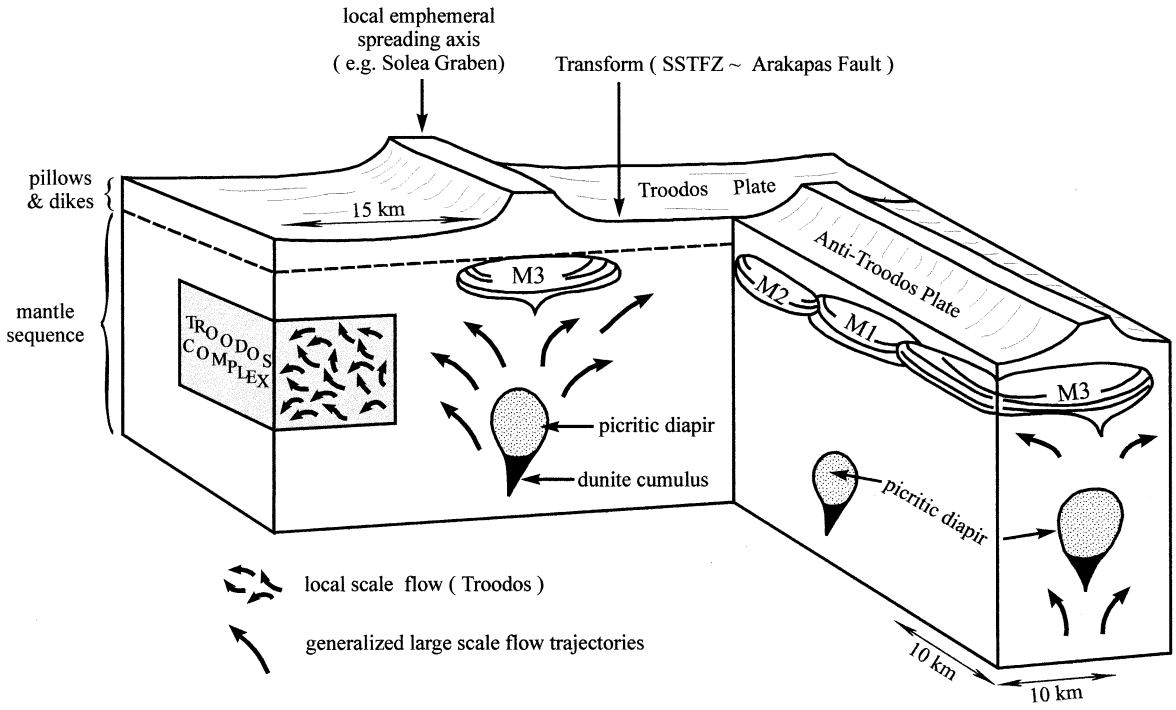

Fig. 2. Schematic model illustrating the location of the Troodos Complex mantle sequence rocks (shaded box) with respect to the Solea Graben spreading axis. Hypothetical, small diapiric bodies yield ephemeral magma chambers (M1, etc.) 10–30 km in diameter, beneath the spreading axis. These are believed to subsequently form the foci from which solid state flow radiates. The shaded box corresponds to the volume of rock whose mineral orientation fabrics are shown from field and magnetic measurements in Figs. 3, 10 and 12 with stereograms of orientation distributions in Figs. 4, 11 and 13.

harzburgites and lhertzolites. Our study concentrated on the highest part of the Troodos range that exposes the deepest parts of the mantle sequence. Sampling concentrated especially on the harzburgites and serpentinized harzburgites (Fig. 3). Although we attempted to identify L–S fabrics in the field, they provided limited data and poor resolution of the fabrics. Also, measurements of the linear and schistose orientations do not readily permit us to quantify the fabric's intensity of development.

In any case, we should recognize that the intensity of the fabric cannot be directly related to the intensity of the causative flow mechanism (stress or strain) because the magnetic fabric arises from several minerals, each of which may have a different alignment mechanism, a different degree of alignment and a different intrinsic magnetic mineral-anisotropy (Borradaile, 1988, 1991; Borradaile and Henry, 1997; Jackson and Tauxe, 1991). These problems have been tackled by Hrouda (1993) and Rochette (1988) amongst others. Moreover, the alignment mechanism for any one mineral varies with conditions (e.g. Nicolas and Poirier, 1976; Poirier, 1985).

The determination of preferred orientation fabrics by conventional petrographic techniques, such as the use of oriented thin-sections or Universal-stage measurements, are time consuming. Moreover, it is very difficult to determine preferred crystallographic orientations for minerals that are optically biaxial or those that possess poor cleavages. Other methods, such as X-ray goniometry, are still more taxing to apply and may be more difficult to interpret.

Rock magnetic methods provide many advantages in the determination of mineral orientation–distributions (Hrouda, 1982; Tarling and Hrouda, 1993; Borradaile and Henry, 1997), in comparison with the aforementioned traditional approaches. When a magnetic field is applied to *any mineral*, it responds by producing an induced magnetization that we measure in dimensionless units of 10^{-6} SI, or μSI, on a volume basis. For mineral separations, it is convenient to quote susceptibility on a mass basis which thus have units of m^3/kg. The latter may be converted to the more commonly used volume units by dividing by the mineral's density (using SI units).

The induced magnetic response always includes an almost negligible diamagnetic contribution due to the induction effect on electron orbits that opposes the applied field (~ -14 μSI). For some rock-forming minerals, this may be the only magnetic susceptibility response (e.g. pure feldspars, calcite, quartz) although inclusions normally raise the susceptibility above the theoretical diamagnetic value. Most rock forming minerals, however, also have an induced magnetic response that enhances the applied field (Table 1). This is a positive, paramagnetic susceptibility that may range up to $+2000$ μSI. Accessory minerals such as iron, titanium and chrome oxides, all present in the rocks studied, respond paramagnetically to low-field susceptibility measurements and have very large susceptibilities (Table 2).

All of these susceptibilities may be measured with such precision that measurements in different directions through

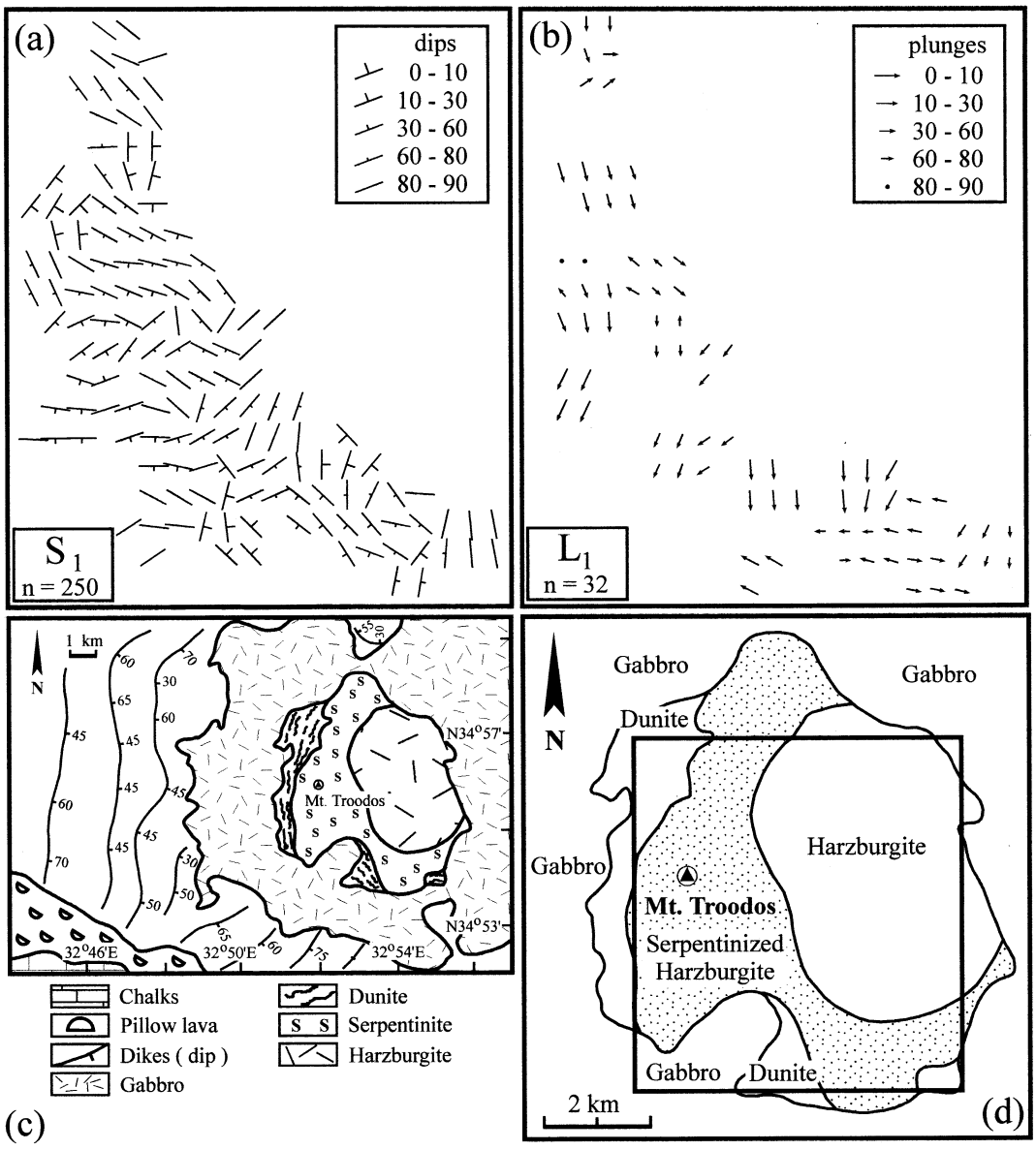

Fig. 3. Field alignments of pyroxene define (a) schistosity (S) and (b) lineation (L) in some harzburgite and serpentinized harzburgite outcrops. The directions have been spatially averaged in 300×300 m^2 subareas, using the Spheristat program of Pangea Scientific. Measurements were weighted according to the inverse of their distance from the center of the square in which the appropriate symbol is plotted. The same averaging process is used for the maps of magnetic anisotropy directions. The heterogeneity of the fabric orientations at the subarea scale is clear. The maps below indicate the geology (c) and the sampled area (d).

a sample yield the magnetic anisotropy, revealing the crystallographic alignment of the constituent grains. The procedure uses a rock sample, prepared in the form of a drill core 25 mm in diameter and 22 mm high, as in paleomagnetic studies. We collect oriented hand-samples in the field, reorient them in the laboratory in a three-axis tilting vice and drill their cores in geographical coordinates. This produces superior results to drilling on outcrop because of improved precision in orientation, reduces logistical problems (supply of gasoline, water) and permits a more effective use of field-time. The archived samples are then readily used in future work, without reference to unique orientations, or unique orientation-conventions. The induced magnetization of the core is measured in seven directions (Borradaile and Stupavsky, 1995) from which the anisotropy of the sample is calculated. This represents the anisotropy of the sample's susceptibility to an ephemeral, induced magnetization. The complete anisotropy measurement and calculation requires about 3 min per sample with the computer-interfaced SI2B equipment of Sapphire Instruments, producing a precision of ~0.1 μSI for routine work.

The magnetic anisotropy is measured in a low field (~0.1 mT), to ensure the linear response of any minor mineral phases that can retain a remanent magnetism, as discussed below. This is usually termed the anisotropy of

Table 1
Magnetic susceptibilities of rock-forming minerals from Troodos

Sample		Low-field susceptibility	Susceptibilities from hysteresis studies		Theoretical paramagnetic susceptibility[a]
		k_{mean} (μSI)	k_p (m^3/kg) × 10^{-9}	k_f (m^3/kg) × 10^{-9}	(μSI)
Pyroxene	1	3629	231	152	523[b]
	2	4521	315	3696	
	5	2080	194	3141	
	6	6605	170	1093	
Serpentine	1	7067	228	2646	
	2	22907	475	30463	
	3	2094	658	21665	112[c]
	4	9870	248	3491	105[c]

[a] Calculated with Syono's (1960) formula from microprobe analysis:

$k_p = d(25.2\ Fe^{2+}\% + 33.4\ Fe^{3+}\% + 33.8\ Mn^{2+}\%)\ \mu SI$,

where 3.47 and 2.61 were average densities (d) for pyroxene and serpentine samples, respectively.
[b] Estimation of Fe^{3+} from microprobe analysis follows the procedure described by Droop (1987).
[c] Droop (1987) Fe^{3+} estimation procedure cannot be used because H_2O content of serpentine cannot be detected by microprobe analysis. Therefore, Syono's formula was modified to $k_p = d(33.4Fe^{3+}\% + 33.8Mn^{2+}\%)$ μSI since Fe^{3+} predominates in lizardite, the type of serpentine here.

magnetic susceptibility (AMS), and it is represented by a second order tensor that may be visualized in the form of an ellipsoid. For many minerals, there is a one-to-one correspondence of longest, intermediate and shortest axes of the AMS ellipsoid with their crystallographic axes, with due allowance for some departure due to crystal-symmetry (e.g. Borradaile and Werner, 1994; Lagroix and Borradaile, 2001). Thus, the AMS ellipsoid loosely defines the orientation distribution ellipsoid of the predominant mineral, usually the one that is most abundant, most anisotropic magnetically and best aligned. The challenge is to derive this from the magnetic susceptibility (e.g. Hrouda and Schulmann, 1990). Notable exceptions occur for some minerals of low symmetry and for those in which the relative magnitudes of maximum, intermediate and minimum susceptibility do not correspond one-to-one with the grain-dimensions (e.g. 'inverse fabric' minerals such as tourmaline, single domain magnetite, etc; Rochette et al., 1992; Lagroix and Borradaile, 2001). With most silicate minerals, such as those studied here, the long axis of the AMS ellipsoid is parallel to the longest dimension of the crystal. Normally, two or more minerals contribute almost equally to the AMS, as in the lhertzolites studied here, and each has an imperfect orientation distribution, and these may differ. Thus, it is not possible to isolate the contribution of individual silicate minerals to the flow fabric. Nevertheless, AMS provides a three-dimensional description of the mean orientation of all silicates (here pyroxenes and olivine). The silicate fabric is quite well defined because several hundred grains occur in each typical core sample of 11.5 cm^3.

In our samples, the largest contribution to the bulk susceptibility is provided by accessory minerals that have very high susceptibilities. These include magnetite, ilmenite, chromite and, rarely, titanomagnetite (Table 2). Although magnetite dominates the bulk (= mean) susceptibility of samples, its shape-controlled anisotropy is so low that ≥40% of a sample's AMS is due to the crystallographically-controlled silicate anisotropy, which is intrinsically high (Borradaile, 1987; Borradaile and Henry, 1997). It is commonly found that high anisotropy mafic silicates dominate the AMS of samples whose mean susceptibility is nevertheless dominated by low-anisotropy magnetite (Borradaile and Henry, 1997; Lagroix and Borradaile, 2001). Occasionally, traces of ilmenite are present, but its Curie point is −218°C so that it responds

Table 2
Magnetic susceptibilities of accessory minerals from Troodos

Mineral	Low-field susceptibility	Susceptibilities from hysteresis studies	
	k_{mean} (μSI)	k_p (m^3/kg) × 10^{-9}	k_f (m^3/kg) × 10^{-9}
Magnetite	6,200,000[a]	–	–
Ilmenite	9890	–	–
Chromite	7540[a]	118	232

[a] Published data from Carmichael (1982).

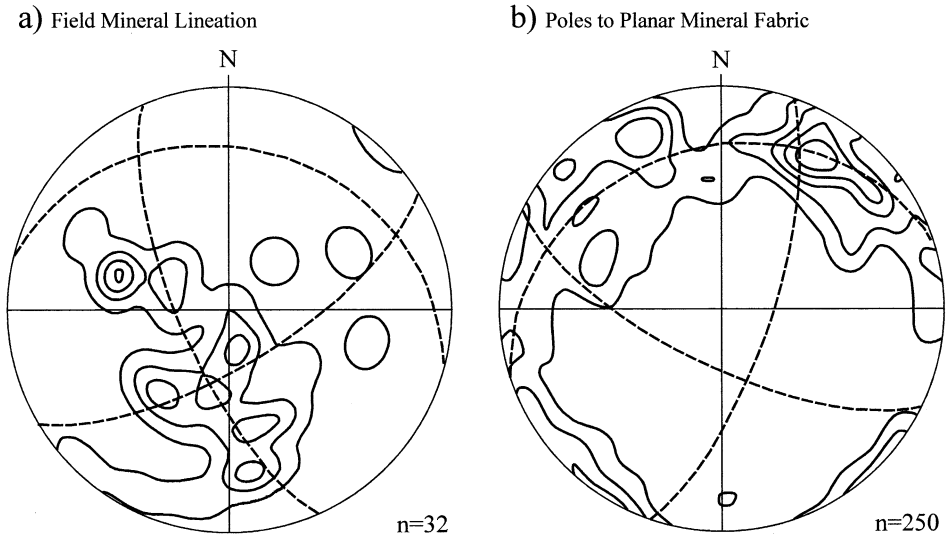

Fig. 4. Lower hemisphere stereogram of all field measurements of L and S. Contours are at multiples of the expected count-concentration for a uniform distribution over the sphere. Dashed lines intersect at the Eigen directions of the orientation distribution. There are relatively few measurements from which to draw conclusions, especially of mineral lineation (a). The poles to S might be bimodal, but a generally S- or E-dipping schistosity may be assumed. This foliation is mostly defined by cataclastic textures and differs in orientation form the penetrative mineral-orientation fabrics revealed by magnetic anisotropy.

paramagnetically at surface/laboratory temperatures and has the same significance as rock-forming silicates for magnetic fabric studies.

As the stress-fields driving the solid state flow were almost certainly non-coaxial, we should not expect parallelism of the older, higher temperature, silicate fabric and younger, lower temperature oxide fabrics. It is therefore important to isolate their contributions to obtain a clear picture of the flow fabric at different stages.

Fortunately, we can distinguish the orientation distribution of grains that carry a remanent magnetization, like magnetite, the most common and significant remanence-carrier. The procedure is somewhat more involved than AMS determination and takes about 20 min per sample. An artificial laboratory magnetization, an anhysteretic remanence (ARM), is applied to the sample using a specially adapted alternating field demagnetizer. The remanence acquired represents the ease of remanence acquisition in that direction. This procedure is repeated in seven different directions, each time erasing the pre-existing ARM by static three-axis AF demagnetization. From the matrix of measurements we determine the anisotropy of anhysteretic remanence (AARM) that is represented by an ellipsoid, just as with AMS. Further details of the procedures and precautions may be found in Jackson (1991), McCabe et al. (1985) and Werner and Borradaile (1996). AARM is almost entirely dictated by the orientation distribution of magnetite in our rocks. Thus, we obtain a separate picture of magnetite grain-fabric versus that of the combined silicate-magnetite fabric provided by AMS. Unfortunately, it is rarely possible to subtract the tensors [AMS] − [AARM] to isolate the silicate fabric from the bulk response of the whole rock (AMS), and the present data would certainly not justify such an approach (Borradaile et al., 1999; Hrouda et al., 2000). As we shall show below, however, using discrete differences in fabric orientations, a qualitative separation is possible by inspection of the stereonets.

2. Results

The sampling area includes harzburgites and serpentinized harzburgites in an area of about 100 km^2 near Mount Troodos, also known as Mount Olympus (Figs. 2 and 3). Strong relief permitted sampling over ~400 m in the vertical direction. Our preliminary survey involved the collection of field measurements of the schistosity and lineation defined by the usually weak-preferred orientation of the elongate mineral grains, chiefly pyroxene and olivine. The latter mineral is extensively altered to iddingsite. The alignments postdate the primary chromite layering in many instances. For this reason, the preferred orientations are attributed to solid-state deformation. Petrographic evidence reveals that this was achieved by cataclastic flow, in some cases utilizing serpentinized microfracture surfaces. Some outcrops are intensely net-veined by serpentine.

Thirty-two outcrops yielded measurable mineral lineation orientations and 250 outcrops permitted measurements of schistosity orientation. The field lineation and foliation are defined principally by the alignment and cataclastic-elongation of pyroxene grains, cataclastic foliae and spaced, serpentinized schistosity planes. As with subsequent directional data for magnetic fabrics, the field fabric orientations were averaged over 300×300 m^2 and the symbol representing the mean is plotted at the center of the square.

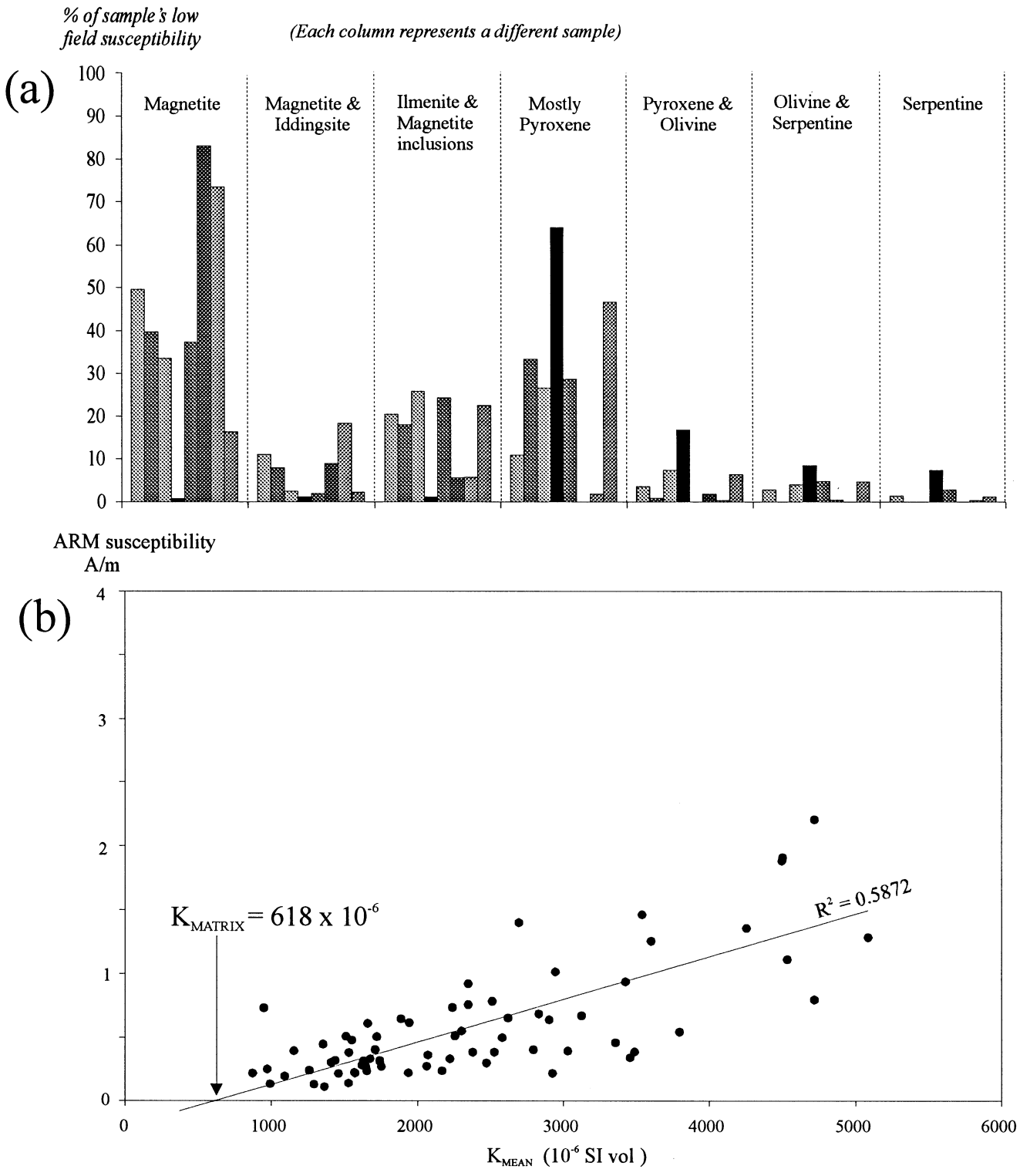

Fig. 5. (a) Partitioning of bulk susceptibility between different mineral separations. Each histogram column represents a different sample. The crushed samples were separated magnetically and by sodium polytungstate heavy fluid solution. The principal contributions to susceptibility in decreasing order of significance are, magnetite, ilmenite, pyroxene and olivine. Olivine cannot be isolated in mineral separations and is heavily altered to iddingsite. Serpentine is also a significant alteration product. Magnetite and ilmenite are accessory minerals. (b) The mean anhysteretic remanence of the samples (ARM susceptibility) reflects the content of remanence-bearing phases. Its correlation with the mean low field susceptibility (k), significant at the 95% level, indicates that remanence is due to a single mineral (King et al., 1982). The theoretically predicted matrix susceptibility is 618 μSI, where ARM is ~0.

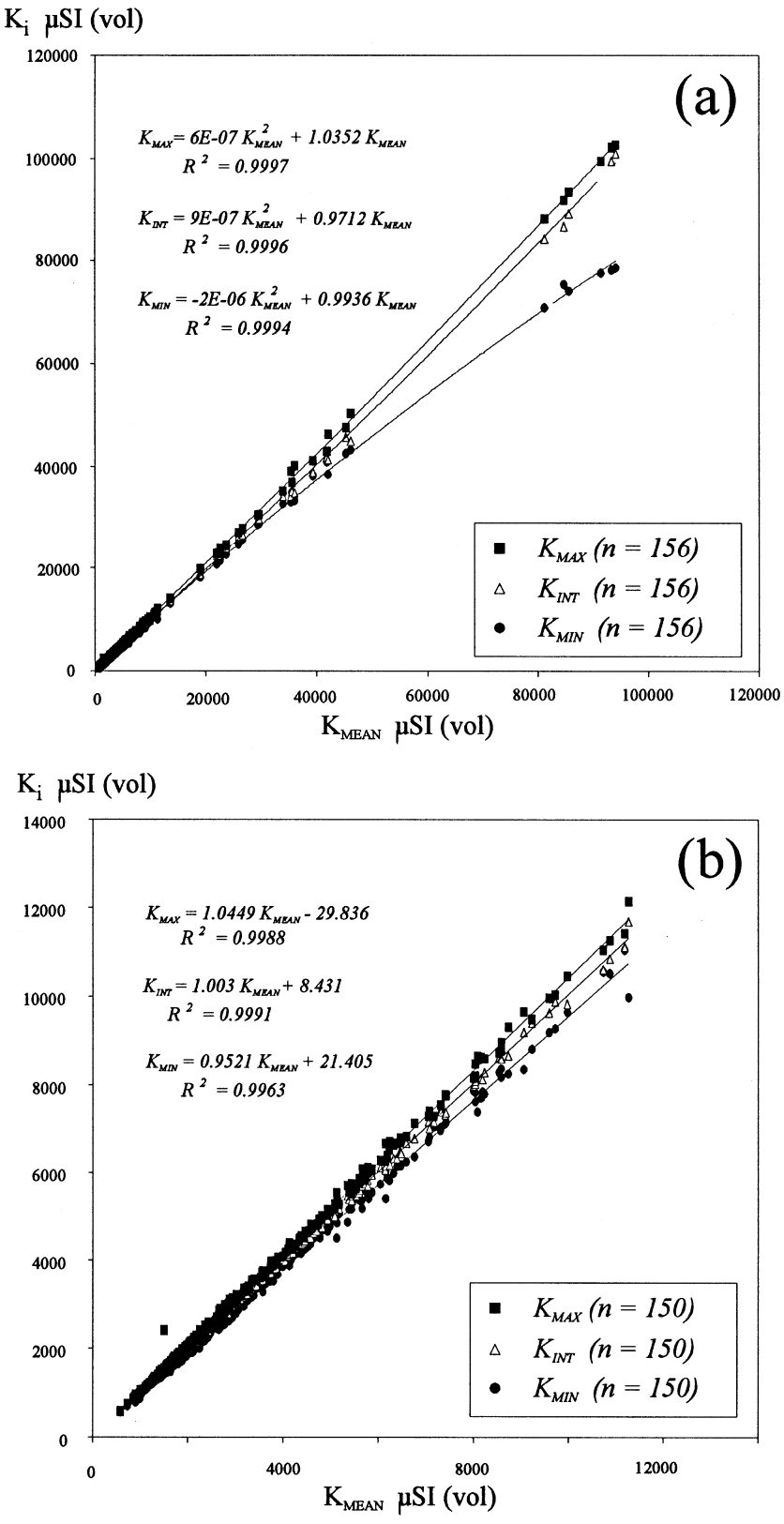

Fig. 6. Principal susceptibilities of Troodos harzburgites plotted against the mean susceptibilities for 156 samples. (a) Total sample shows a non-linear mixing relationship. (b) Exclusion of high susceptibility outliers yields a linear relationship that Henry (1983) showed may result from the mixing of two phases, a silicate matrix and a dilute high susceptibility phase (magnetite). The simultaneous solution of the three regression lines predicts an estimated matrix susceptibility of 683 µSI (cf. 618 µSI by King's method of Fig. 5b).

Outcrop measurements were weighted according to the inverse of their distance from the center of the square in which the symbol is plotted. This procedure and subsequent stereogram contouring was made possible using Spheristat software marketed by Pangea Scientific (Canada).

The field measurements show spatial heterogeneity in the flow pattern at the scale of many outcrops (Fig. 3). Areas of several hundred metres square may have similar field L–S fabrics that merge into different orientations in adjacent subareas. Thus, subareas of approximately $300 \times 300\ m^2$ are sufficiently small to be considered homogeneously strained but adjacent subareas commonly reveal different mean fabric orientations. Over the whole region, however, a consistency reappears (Fig. 4), with mineral lineations plunging gently southwards and westwards. The S-component is still better defined regionally, dipping SW, as shown by the strong maximum. Nevertheless, the field foliation disperses to southerly and south-easterly dips. This may be attributed to the later doming of the harzburgite just southeast of the sampled area (Fig. 3), shown by the regional deflection of stratified rocks, pillow lavas and dikes about the Troodos mountain range.

3. Magnetic mineralogy

The interpretation of magnetic anisotropy requires a knowledge of the minerals, their types of magnetic response, their anisotropies and their proportions in the rock. Only after an evaluation of this information can one deduce the minerals' orientation distributions from magnetic anisotropy of the sample. More sophisticated approaches exist that may permit greater depth of analysis than presented here, but they are impractical, as yet, for routine petrofabric studies of large sample-suites (e.g. Rochette and Fillion, 1988; Richter and van der Pluijm, 1993).

We have applied the techniques of Borradaile et al. (1987, 1990) to determine the susceptibility contributions of the different minerals in our rocks. Using a combination of magnetic and density separation, and hand-picking we determined the fractional contribution of our rock-forming minerals to bulk susceptibility as shown in Fig. 5a. The matrix is composed of cataclastically deformed olivine and orthopyroxene. The susceptibilities of these fractions are very high, averaging $15 \times 10^{-6}\ m^3/kg$; assuming densities of $3300\ kg/m^3$, this corresponds to volume susceptibilities of ~49,500 μSI. The role of inclusions is confirmed where separate crystals of serpentine and orthopyroxene were measured with susceptibilities well above the paramagnetic levels (<2000 μSI) expect for mafic silicate-lattices (Fig. 5a; Lagroix and Borradaile, 2001). Rochette (1994) notes that serpentinite is one of the most susceptible rocks of the earth. As he notes, however, this is largely due to the role of accompanying magnetite, an abundant byproduct of serpentinization (Dunlop and Özdemir, 1997, p. 404). Mean anhysteretic remanence (ARM) reflects only the content of 'ferro'-magnetic phases such as magnetite in this study. Plotting ARM versus low field susceptibility for each sample produces a linear relationship (Fig. 5b), where one remanence-bearing phase dominates (King et al., 1982). Moreover, projecting the regression line back to zero-remanence predicts a paramagnetic-matrix susceptibility of 618 μSI which is a reasonable value for pyroxene or most other mafic silicates, *neglecting any inclusions*. It was not possible to isolate the bulk low field susceptibility contribution of olivine because it is extensively altered to iddingsite.

An alternative evaluation of susceptibility contributions may be achieved using anisotropy and bulk susceptibility data. Henry (1983) showed that, under certain simple commonly recognized constraints, the mixing of a high with a low susceptibility phase yields linear relationships between K_i and K_{mean} where $i = 1,2$ or 3 for maximum, intermediate or minimum principal susceptibility. This model works well in many simple systems that can be regarded as two-components from the point of view of mineral susceptibility and anisotropy (Borradaile and Henry, 1997). In the Troodos harzburgites such a plot is not linear (Fig. 6a). This may be due to the mixing of three different phases, of distinct mean susceptibilities. It is also true, however, that the lithologies and fabrics are neither as uniform nor as simple as those normally treated by the method of Henry (1983). We propose that the significant contributions from magnetite (>2,000,000 μSI), ilmenite (~400,000 μSI) and ferromagnesian silicates (<2000 μSI) yield a more complex mixing model. This is confirmed by excluding the samples in which magnetite and ilmenite are significant and competitive, (i.e. $K_{mean} > 14{,}000$ μSI) because the remaining data then conform to the linear Henry-model (Fig. 6b). The simultaneous solution of the three regression lines should fix the mean susceptibility of the silicate lattices in the matrix: for our data this is 683 μSI, 11% higher than the value predicted by the method of King et al. (1982), shown in Fig. 5b. In view of the nature of the assumptions in both methods this is a satisfactory indication that the silicate matrix, excluding inclusions, has a susceptibility of ~650 μSI.

Hysteresis measurements confirm the behaviour, and relative importance of the accessories that behave ferromagnetically (*sensu lato*). A Princeton Measurements Micromag 2900 instrument provided hysteresis loops for silicate mineral grains of a few milligrams. Above 0.4 T, the remanence is saturated and the loops show a horizontal portion, parallel to the field axis. By rotating the saturated parts of the loops, we corrected for the non-ferromagnetic response of the matrix. For these rocks, the slope correction yields a paramagnetic (positive) susceptibility. We normalized this by mass to yield mass susceptibilities in units of m^3/kg. The gradient of the rotated loop, near the origin, then approximates the low-field

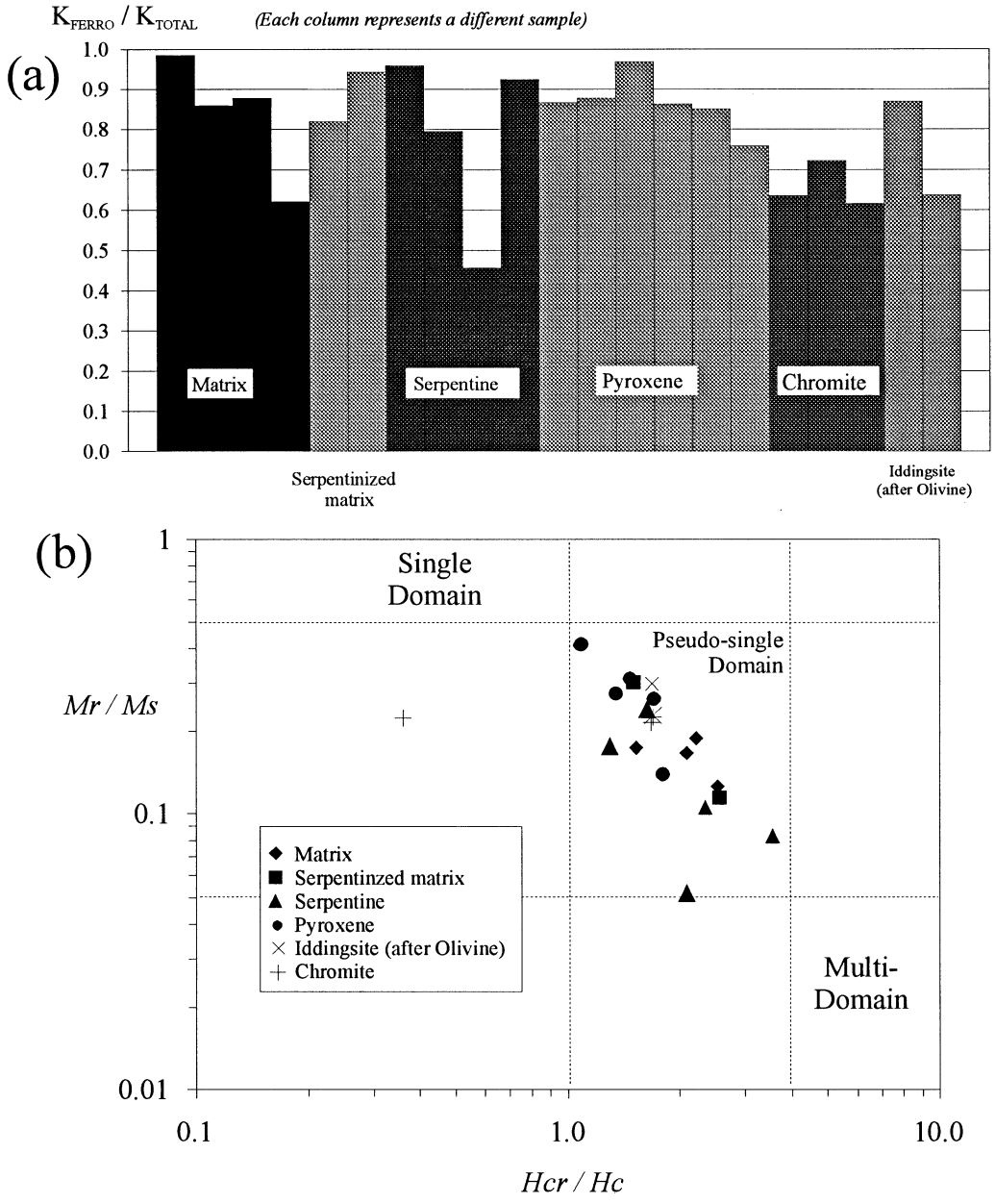

Fig. 7. (a) From hysteresis loop determinations, the paramagnetic and 'ferromagnetic' components to the bulk susceptibility were isolated. The ferromagnetic component of the total susceptibility generally exceeds 60%; however, the magnetite is both an accessory and an inclusion in silicates. Each column of the histogram represents a different sample. (b) Hysteresis parameters on the plot of Day et al. (1971) show that the inclusions in orthopyroxene and of the alteration products iddingsite (after olivine) and serpentine, and cataclastic matrix (mostly orthopyroxene, serpentinized olivine) all respond as pseudo-single domain (PSD) magnetite. M_r/M_s = zero field remanence saturation remanence ratio; H_{cr} = coercivity of remanence, H_c = coercivity.

susceptibility of the ferromagnetic inclusions (e.g. Borradaile and Werner, 1994).

'Ferromagnetic' behaviour contributes more than 50% of the bulk susceptibility in most samples and is chiefly attributable to inclusions in silicate, especially serpentine (Fig. 7a). Combining the main hysteresis parameters on a combination of traditional plots (Wasilewski, 1973; Day et al., 1977) as shown by Borradaile and Lagroix (2000), reveals the type of magnetic response of the magnetite inclusions. Here, we simply show the traditional plot of Day et al. (1977) in Fig. 7b. The hysteresis properties correspond to pseudo single domain (PSD) magnetite, in the rock-matrix, in the serpentine and pyroxene monocrystals, and in the iddingsite pseudomorphs after olivine. Acquisition of isothermal remanence confirms this. Although visible magnetite in the samples should respond as multidomain magnetite, cataclasis may cause it to respond similarly to finer-grained magnetite. Jackson et al. (1993) explain this by 'magnetic hardening'; a reduction in *effective* magnetic grain-size due to the increase in

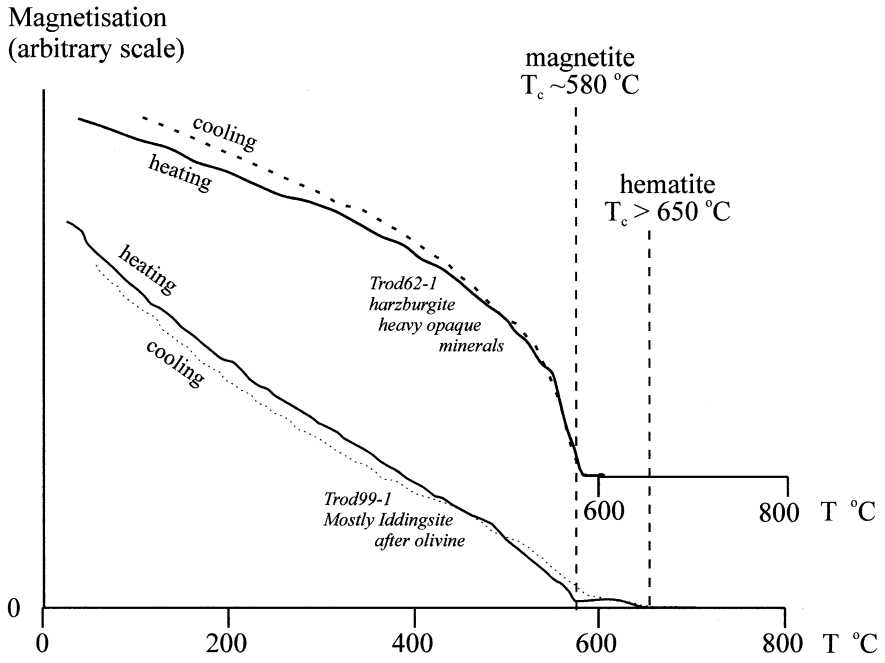

Fig. 8. Curie balance tests on two representative heavy mineral separations from Troodos harzburgites. Most magnetic fractions show a Curie point corresponding to magnetite. Iddingsite alteration after olivine carries accessories that show Curie points corresponding to magnetite and hematite.

dislocation density. In PSD–MD magnetite, maximum and minimum susceptibilities correspond, respectively, with the maximum and minimum dimensions of grain shapes. This is an important consideration, because SD magnetite reverses the association, resulting in inverse fabrics (Rochette, 1987; Rochette et al., 1992). Still worse, mixtures of SD and PSD/MD behaviour cause intermediate situations between entirely inverse and entirely normal fabrics.

Thermomagnetic tests using a translational-style Curie balance (Sapphire Instruments) identify the average Curie temperature of the main remanence-bearing phase at 585°C ($n = 8$) in all samples (Fig. 8). This confirms the magnetite as the main remanence carrier. Occasionally, a lower Curie temperature of ~350°C suggests the presence of a titanomagnetite. All mineral separations reveal the presence of magnetite, indicating that it is a ubiquitous accessory mineral or inclusion. Iddingsite alteration after olivine carries magnetite and hematite in most cases.

4. Anisotropy of magnetic susceptibility (AMS)

AMS is the most common type of magnetic anisotropy that is measured. The fabric ellipsoid represents an average alignment of all minerals in a core sample of ~11 cm^3 summarizing the effects of the orientation distribution of several hundred mineral grains in most samples. The anisotropy ellipsoid provided by this attractive technique should not be interpreted directly as an orientation–distribution ellipsoid, unless the rock is monomineralic. Different minerals have different bulk susceptibilities, and different susceptibility-anisotropies. Thus, even if they all have the same orientation distribution, the interpretation of the sample's anisotropy requires an understanding of the partitioning of susceptibility, and anisotropy, between the different phases. The interpretation may be very complicated where each mineral phase has a different orientation distribution.

AMS is usually the only type of magnetic fabric measured and, as we suggest, without an appreciation of magnetic-mineralogy it may be misleading (Rochette et al., 1992; Borradaile and Henry, 1997). For example, consider a hypothetical sample comprising 99% amphibole with a bulk susceptibility of 3000 μSI and 1% magnetite with a bulk susceptibility of 3,000,000 μSI. Moreover, let us hypothesize that the amphibole is well aligned with its maximum susceptibility axis north–south, whereas the magnetite has a younger east–west magnetic lineation. The high susceptibility of the accessory magnetite would dwarf the susceptibility of amphibole by almost 10:1. Even allowing for a greater susceptibility-anisotropy of the amphibole due to crystallographic controls, versus the lower shape-controlled AMS of magnetite grains, the magnetite's orientation–distribution dominates the sample's fabric. Thus, the whole-rock AMS ellipsoid would define an E–W lineation camouflaging the silicate petrofabric.

For a polymineralic sample with some preferred orientation of minerals, AMS balances the contributions of different proportions of minerals with different bulk susceptibility, different anisotropy and perhaps a different

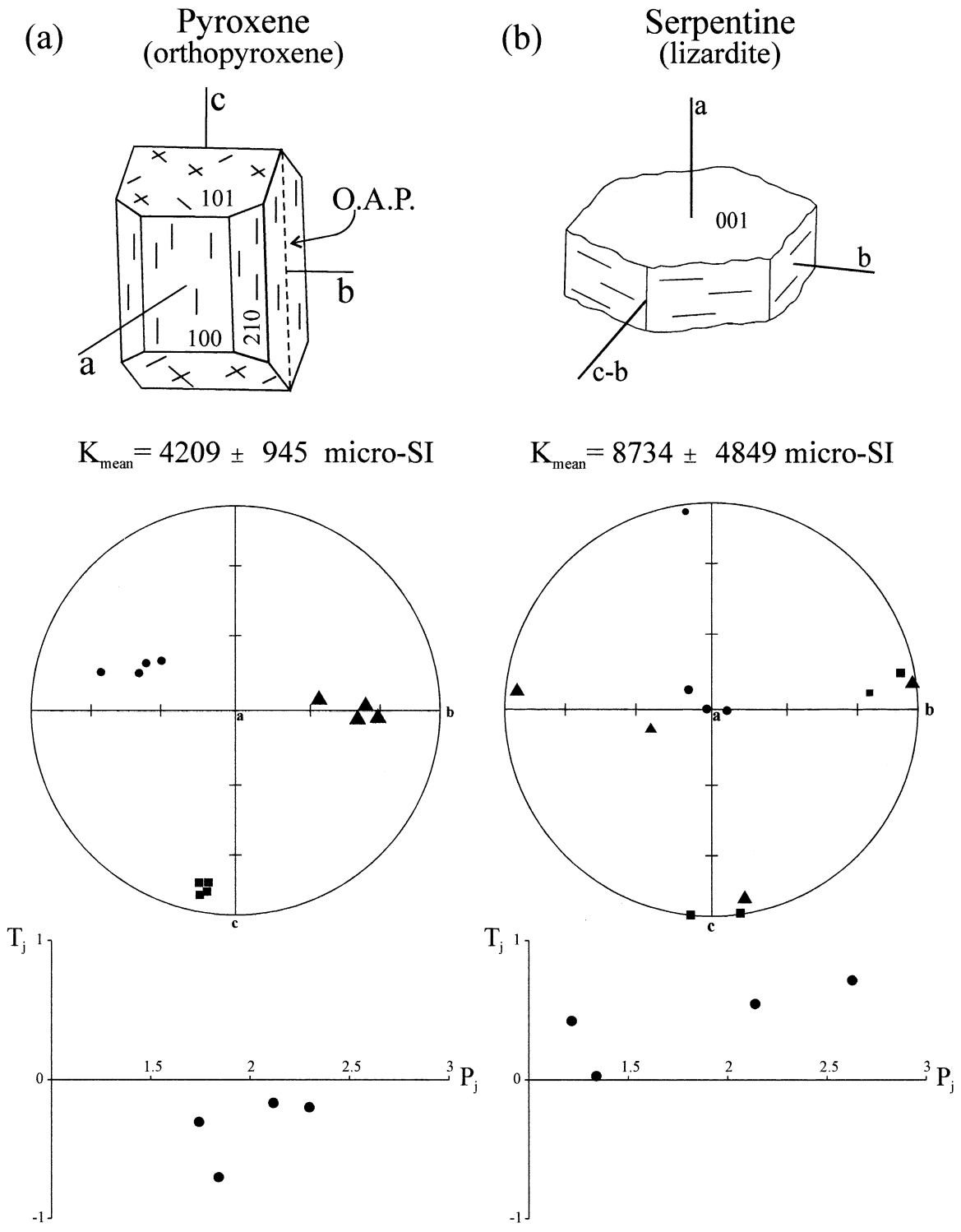

Fig. 9. Crystallographic control of AMS in (a) orthopyroxene and (b) serpentine crystals from Troodos. The mean susceptibilities far exceed that expected for the silicate lattice (<1000 μSI), indicating the presence of iron oxide inclusions. Nevertheless, the silicate host retains some crystallographic control on the principal susceptibilities with k_{max} parallel to *c* in pyroxene and in most serpentines. k_{min} is parallel to *a* in serpentine but oblique in pyroxene.

degree of preferred orientation. Although accessory magnetite contributes much to the bulk susceptibility, it normally contributes less to the AMS than the more anisotropic, but lower susceptibility silicates (Borradaile, 1987, 1991).

The correspondence of susceptibility-axes and grain-morphology must also be considered. Due to high susceptibility and low magneto-crystalline anisotropy, the AMS of a *multidomainal* magnetite grain is defined by its shape. Thus, there is a one-to-one correspondence of maximum, intermediate and minimum susceptibilities with grain

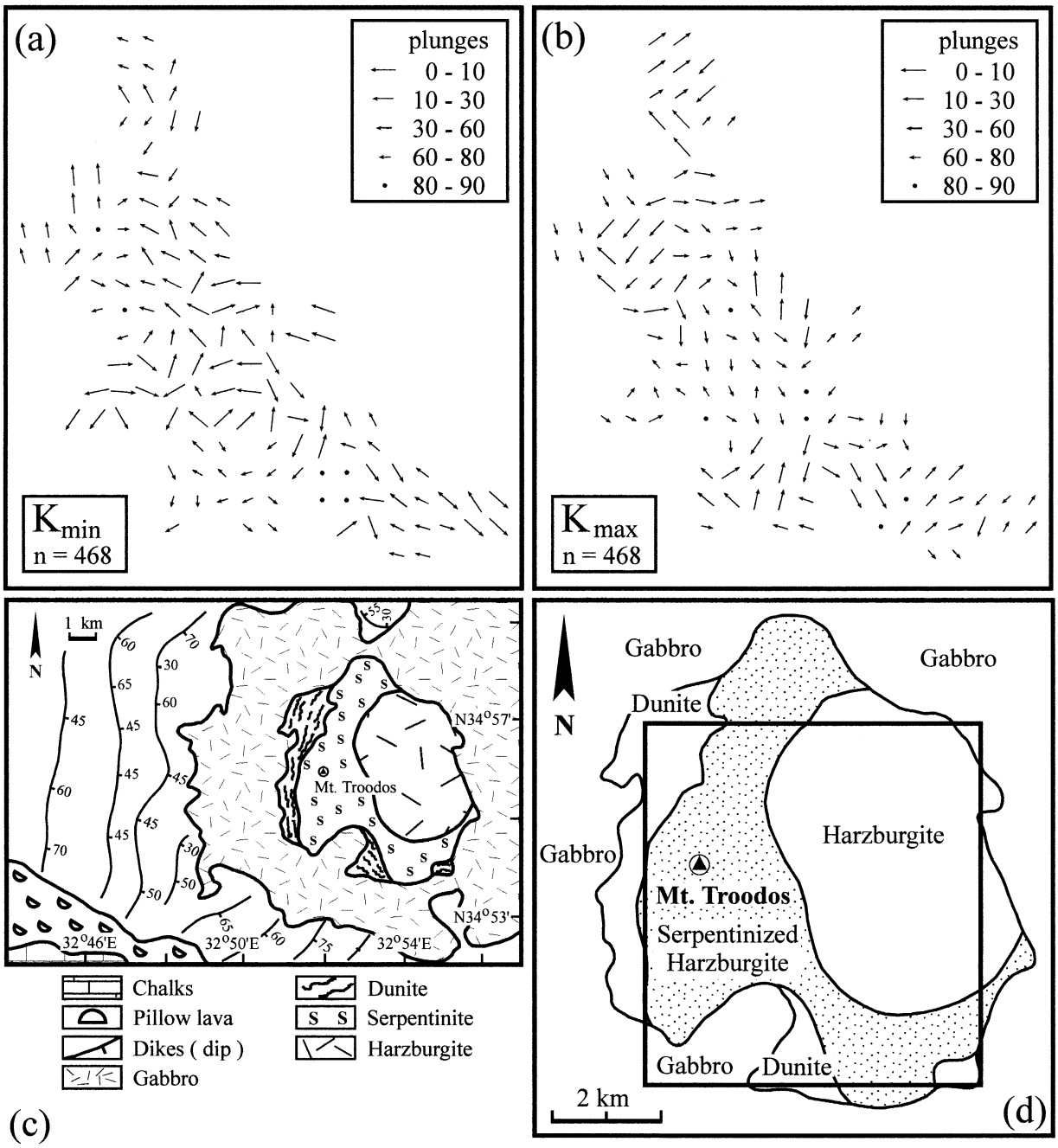

Fig. 10. Map distribution of maxima and minima of low field susceptibility anisotropy (AMS). The directions have been spatially averaged in 300×300 m^2 subareas, using the Spheristat program of Pangea Scientific. Measurements were weighted according to the inverse of their distance from the center of the square in which the appropriate symbol is plotted. K_{min} represents the pole to magnetic foliation. AMS represents the average alignment of all minerals, but chiefly from almost equal contributions due to magnetite and pyroxene. The AMS contribution of silicates is due to their crystal preferred orientation whereas the AMS contribution of magnetite derives from its dimensional preferred orientation, or shape-fabric.

dimensions. For all other minerals, however, AMS is defined by crystallography and the anisotropy of some silicates may be quite high (Borradaile and Werner, 1994; Borradaile and Henry, 1997).

The determination of AMS for individual minerals is taxing, and a variety of procedures have been attempted. In our case, the large grain size of the rocks made it possible to determine AMS of single grains either with a conventional susceptibility meter, or by processing hysteresis loops obtained using the Micromag instrument. Mafic monocrystals from Troodos invariably have large susceptibilities that can only be explained by the contributions from ferromagnetic inclusions. Nevertheless, the AMS of most orthopyroxene and serpentine monocrystals is still controlled by their crystallographic symmetry (Fig. 9). Thus, the magnetite inclusions must be oriented so as to

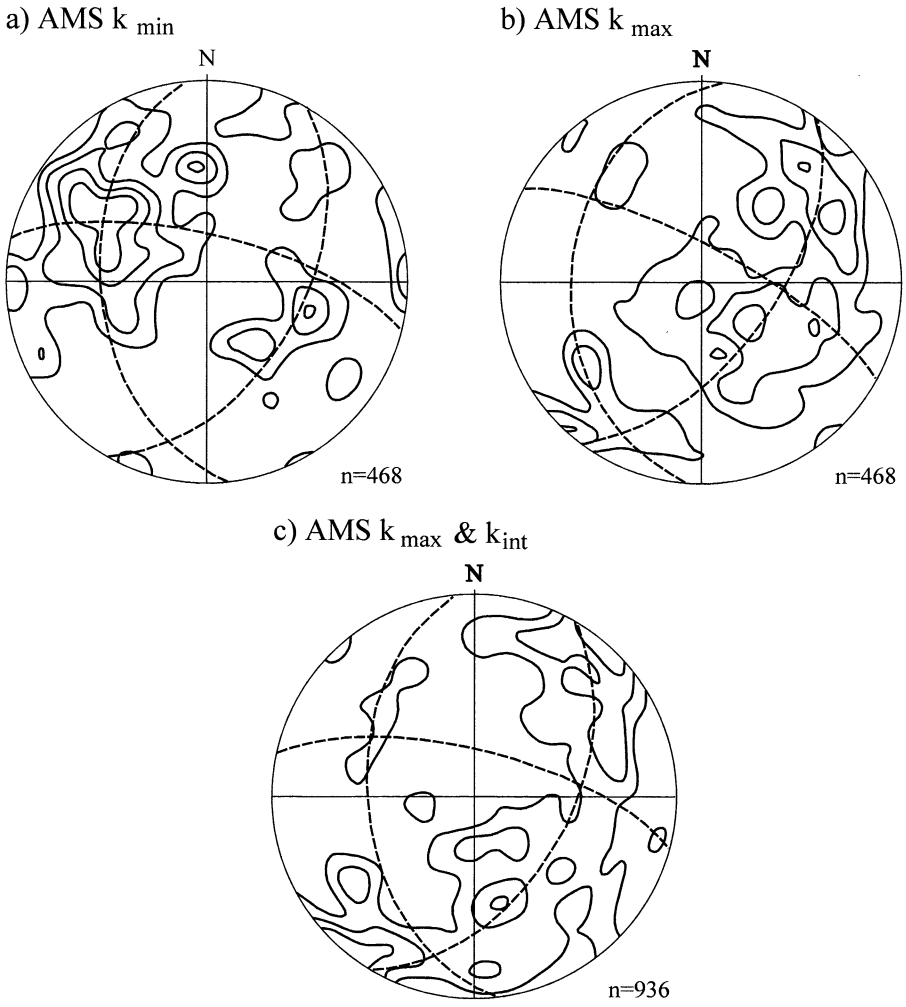

Fig. 11. Lower hemisphere stereograms of principal directions of low field magnetic susceptibility (AMS). This sums the induced magnetic response from all minerals in the sample. Contours are at multiples of the expected count-concentration for a uniform distribution over the sphere. Dashed lines intersect at the Eigen directions of the orientation distribution. (a) Minimum susceptibilities, the poles to the 'magnetic foliation'. Thus the average AMS foliation dips SE. (b) Maximum principal susceptibility directions that disperse over the girdle defined by the magnetic foliation. There are two clusters in the distribution, one plunging steeply SE and another plunging gently ENE: the former corresponds to a cluster of AARM maxima (see Fig. 13b). (c) Combined maximum and minimum AMS axes define a broad girdle that provides an alternative definition of the magnetic foliation, whose pole is defined by the cluster of minimum axes in (a).

enhance the host-silicate's intrinsic AMS signal. The low symmetry of clinopyroxenes prohibits a similar assessment. Table 1 summarizes our estimates of the mineral-AMS values and, by contrast, Table 2 shows values for the accessory minerals.

The rocks' AMS balances contributions from the silicate fabric and the less anisotropic accessory magnetite because the latter forms ~41% of the bulk susceptibility (Fig. 7a). Measurements of AMS orientations considerably exceed the number of field-fabric measurements, e.g. for 250 field foliations and 32 field lineations there were, by comparison, 468 complete specifications of the three AMS directions. Thus, one can place much more confidence on the interpretation of spatial distributions (Fig. 10) and orientation distributions (Fig. 11) of magnetic fabrics. The ubiquitous success of AMS fabric measurement is one of its greatest merits. As with field measurements (Fig. 3), the AMS fabrics show a spatial heterogeneity between 300 m^2 subareas, within which the fabrics are reasonably uniformly oriented. Regionally, however, the mean AMS foliation has a well-defined SE dip (Fig. 11a and c). The AMS lineation is also regionally consistent, but bimodal, with clusters plunging steeply SE and more gently ENE (Fig. 11b). Based on investigations of magnetic mineralogy, we know that magnetite and silicates contribute almost equally to the bulk susceptibility. We shall demonstrate below that one of the AMS orientation-modes is attributable to the magnetite fabric and the other to the silicate fabric.

5. Anisotropy of anhysteretic remanence (AARM)

Unfortunately, many samples were rejected because the sample requirements are more stringent than for AMS

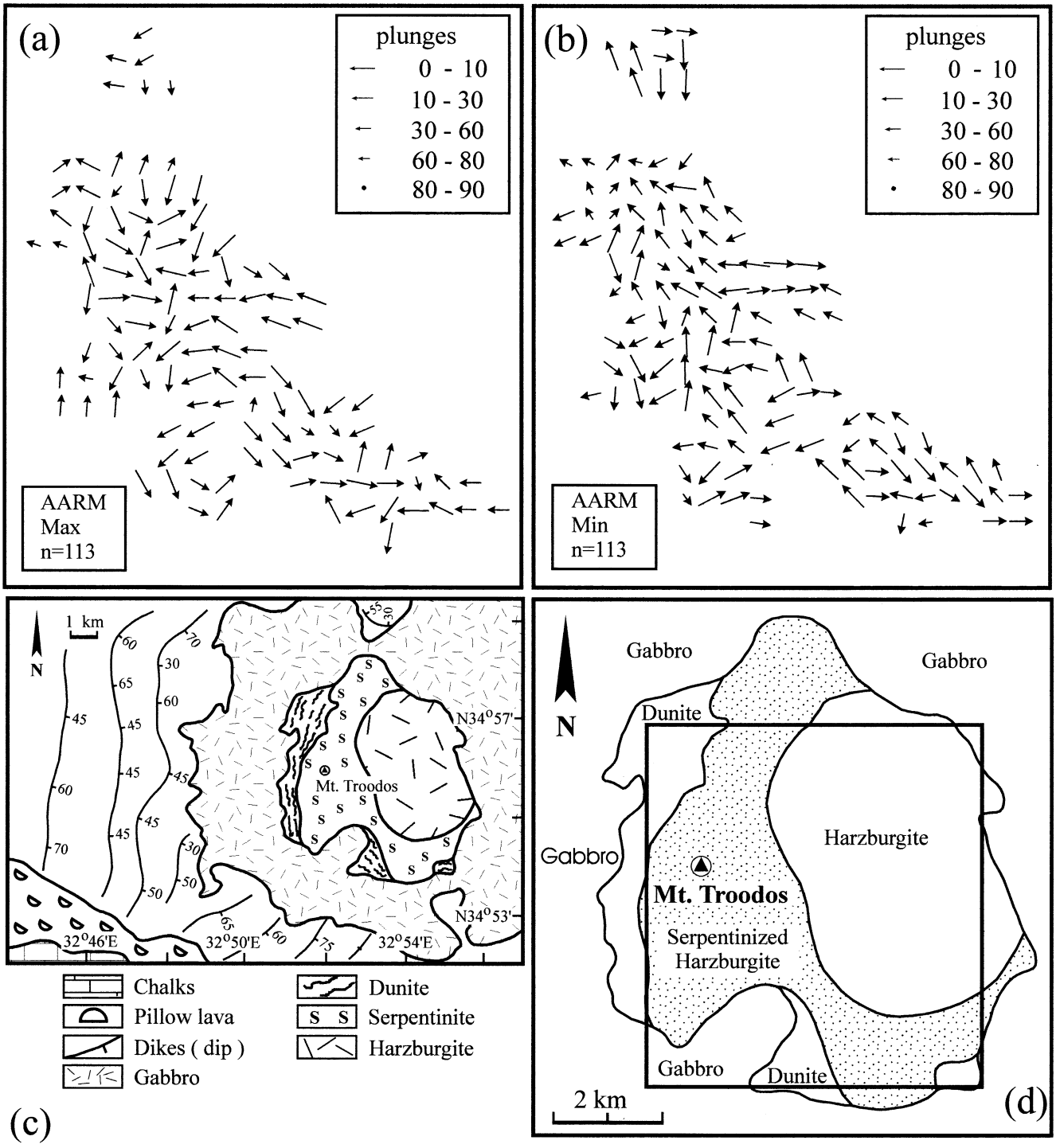

Fig. 12. Map distribution of maxima and minima of AARM. Directions have been spatially averaged in 300×300 m^2 subareas, using the Spheristat program of Pangea Scientific. Measurements were weighted according to the inverse of their distance from the center of the square in which the appropriate symbol is plotted. $AARM_{min}$ represents the pole to foliation. $AARM_{max}$ represents the mineral magnetic lineation which, in the case of magnetite, corresponds to the preferred dimensional orientation, not crystallographic alignment.

measurements. In unsuitable samples, the combination of high anisotropy and high remanence deflected the laboratory magnetizing field far from the intended direction of application. Consequently, the seven remanences applied to those samples fail to conform to the directions required by the tensor calculation. It was only possible to determine AARM for 113 samples.

The spatial distribution of AARM fabrics is less chaotic than for AMS, or for L–S fabrics (Fig. 12). This is mainly because AARM represents the preferred dimensional

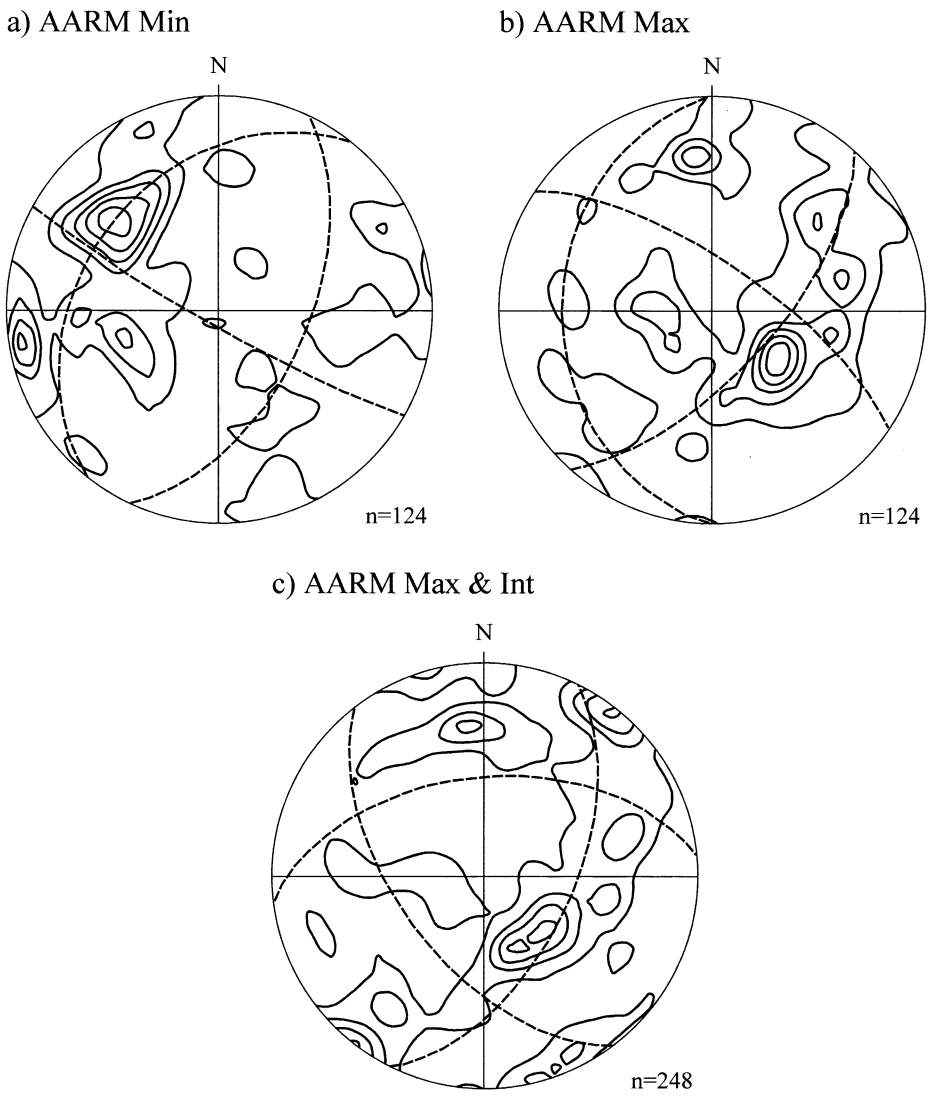

Fig. 13. Lower hemisphere stereograms of principal directions of anhysteretic remanence (AARM). This isolates the orientation distribution of remanence-bearing grains, in this study, magnetite. Contours are at multiples of the expected count-concentration for a uniform distribution over the sphere. Dashed lines define principal planes which intersect at the Eigen-directions of the orientation distribution. (a) The minima-concentration is perpendicular to the 'magnetic foliation' which, in turn, is almost parallel to the AMS foliation (see Fig. 11). (b) The maxima-concentration corresponds to *one* peak of maxima in the AMS distribution (see Fig. 11b). (c) Combined maximum and minimum ARM axes define a broad girdle that provides an alternative definition of the magnetic foliation, whose pole is defined by the cluster of minimum axes in (a).

orientation of magnetite alone but it may also indicate lesser heterogeneity of flow at the late-stage development of AARM. For the PSD-magnetite in these samples, the maximum and minimum susceptibilities correspond to the long and short *dimensions* of multidomainal magnetite grain *shapes*.

AARM principal directions appear stereographically in Fig. 13. A clearly defined AARM foliation (Figs. 13a,c) is approximately parallel to the AMS foliation (Fig. 11a and c). This parallelism at least indicates that the same solid state flow plane constrained orientation–distributions of both magnetite and silicates although magnetite crystallized or recrystallized later, at a lower temperature. Most significantly, however, the AARM maxima, representing magnetite long axes, show a single cluster, dipping steeply SE in the foliation plane. This peak corresponds to one of the two AMS lineation-peaks (Fig. 11b). This reinforces our inferences about the similar but independent contributions of magnetite and silicates to AMS. The differences in the directions of the magnetite grain and silicate crystal long axes can be attributed to their different rheological responses or to later recrystallization of magnetite in a stress field that was gradually changing orientation.

6. Symmetry and intensity of magnetic fabrics

In practice, it is difficult enough to interpret the orientation distributions of AMS principal directions for a *polymineralic, multi-fabric* tectonite. However, the *shapes*

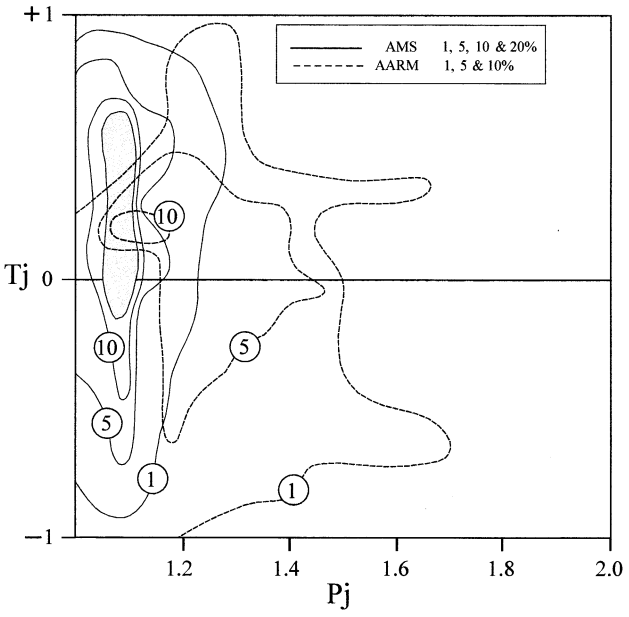

Fig. 14. Jelinek (1981) fabric plot shows the shapes (T_j) and intensity/eccentricities (P_j) of ellipsoids that describe magnetic anisotropy. Note that these describe the shapes of individual anisotropy ellipsoids, which does *not* automatically correspond to the shape of the ellipsoid describing their orientation distribution. $T_j = +1$ for oblate ellipsoids, $T_j = -1$ for prolate ellipsoids, $T_j = 0$ for neutral ellipsoids. $P_j = 1$ for the sphere. The distribution of AARM (magnetite) fabric ellipsoids has a very wide spread, including high intensities with $P_j > 1.5$ in some cases; constricted and disc-shaped fabric ellipsoid types are almost equally common. AMS fabric ellipsoids are more restricted in shape, but still range from rod- to disk-shapes. The intensities are even more restricted, mostly with $T_j < 1.1$. At almost all shape-values (T_j), the same intensities are equally developed (P_j): this suggests the silicate alignment is about as well developed as possible.

of the magnetic fabric ellipsoids are beyond interpretation in these cases. We need only to realize that the AMS ellipsoid shape combines imprecisely known proportions of several different minerals, each with a different mean susceptibility *(ellipsoid-magnitude)*, and different intrinsic mineral-AMS *(ellipsoid-eccentricity)*. Moreover, even if the minerals were perfectly coeval in a coaxial strain history each would show a different degree of alignment according to its crystallographic-symmetry, intrinsic mineral-AMS and the alignment mechanism. There is little hope that we may interpret much from *shape-distribution* data in the near future. Thus, although still useful, shape-eccentricity plots (T_j–P_j, Jelinek, 1981), should probably be restricted to the quantification of the linear versus planar components of the fabric, thus improving upon traditional field estimates of L–S fabric type that are difficult to quantify (e.g. L > S, L = S, etc.). In particular, by comparison with mineral magnetic-anisotropy, one can estimate the degree of perfection of the orientation distribution: a perfectly aligned grain aggregate would show a *saturation* magnetic fabric, with the rock's AMS shape, similar to that of the dominant mineral(s). Fig. 14 shows the shape parameter T_j (+1 = oblate, −1 = prolate) plotted against eccentricity P_j ($P_j = 1$ for a sphere).

AARM measurements of magnetite fabrics show characteristically high intensities ($P_j > 1.5$ in some cases, mean = 1.32). This is primarily due to physical and crystallographic controls and cannot be taken to indicate strong tectonic controls by comparison with the much lower values for AMS. The fabric shape spreads broadly around neutral values ($T_j = 0$). This indicates that the tectonic fabric has relatively little influence in controlling AARM fabric shapes.

AMS fabric shapes are difficult to interpret in terms of preferred mineral orientations because they combine responses from accessory minerals (chiefly magnetite) and silicates. However, intensities (mean $P_j = 1.08$) are lower than for AARM, a commonly recognized rock magnetic feature. The intensities are almost equal at the full range of fabric shapes (T_j) represented by the sample suite. This suggests that fabric intensities are equally well developed at all shapes ranging from the mid prolate ($T_j = -0.5$) to mid oblate ($T_j = +0.5$) fields. This may indicate that silicate crystallographic alignments are optimally developed or *saturated*, a feature commonly recognized in stress-controlled crystallization of plutonic or igneous rocks. These fabric intensities (P_j) may thus approach the intrinsic values for the constituent minerals.

7. Interpretation

Within areas of 300 m^2, the flow of the harzburgites was homogeneous but commonly differs between adjacent subareas (cf. Figs. 10 and 12). This confirms that the scale of heterogeneous solid state flow is at a kilometric-scale. However, for the entire ~100 km^2 sample-area, field L–S fabrics, AMS (silicates + magnetite) and AARM (magnetite) fabrics all indicate a consistently SE-dipping foliation and a southerly or easterly dipping mineral lineation. The field L–S fabrics are least reliable because they are poorly developed or absent. Moreover, they are usually only visible on weathered surfaces where it is difficult to determine the causative mineral. In the field, the L–S fabric is mainly of the planar type with S > L and is clearly cataclastic in character: trains of fractured olivine and pyroxene, and elongate cleaved and altered olivine (serpentinite, iddingsite) defining a shape fabric. The cataclastic flow is clearly a post-magmatic feature, cutting through primary layering defined by chromite and other lithological contacts.

Every sample provides an AMS fabric, and 25% provided an AARM fabric. These precisely defined fabric orientations are principally due to alignments of pyroxene, serpentine (AMS) and magnetite (AARM and AMS). Our studies of magnetic mineralogy show that, on average, ~41% of the bulk susceptibility is due to magnetite and the remainder is due mainly to orthopyroxene, clinopyroxene and serpentine with subordinate contributions

from olivine (mostly altered to iddingsite) and chromite. However, the anisotropy of the magnetite is much lower than for the other minerals so that despite its high susceptibility, magnetite and the silicates contribute approximately equally to the overall AMS signal. From the SE-dipping AMS, AARM and field foliations, we infer that the mean asthenosphere flow was upwards to the NW over the mantle sequence volume of approximately 500–900 km^3 represented by the Troodos range.

The AMS lineation, or maximum susceptibility, has two modes, plunging steeply SE and gently ENE. Their interpretation is made simple because the steep SE lineation corresponds to the single AARM lineation mode that can only be due to the preferred dimensional orientation of PSD/MD magnetite. Thus, we recognize that the magnetite lineation plunges steeply SE and the silicate lineation plunges gently ENE. The earlier, silicate fabric lineation is almost normal to the Solea spreading axis. The later magnetite lineation is oblique, however, indicating a change in flow direction as temperatures fell, and as the material moved further from the spreading axis.

We suggest that the silicate lineation represents WSW-upwards, solid state flow at the top of a small diapir at high temperatures but with a considerable cataclastic component to the deformation mechanism. The dipping foliation indicates proximity to the spreading axis and the obliquity of the early silicate and later magnetite lineations favors a diapir of small diameter (~30 km). The closest local spreading axis, represented by the Solea Graben lies N–S (originally E–W) so that this spreading pattern probably reflects part of a radial flow pattern from a focus SE of Mount Troodos, approximately 5 km south of Pano Amiandos (Fig. 1). From studies of other ophiolites, it is now believed that flow patterns, *in detail*, are not simply perpendicular to spreading axes but radiate from small centers of solid state and magmatic diapirism (Cueleneer et al., 1988; Gass et al., 1994). We may infer that this late stage solid state flow was at a high temperature but it was nonetheless partly cataclastic. The magnetite appears to have crystallized or recrystallized at lower temperatures when a different stress regime prevailed. The steeper orientation may indicate the effects of uplift and radial expansion of the diapir during late serpentinization. The focus of uplift would have been also located somewhere SE of Mount Troodos.

Our observations are compatible with the hypothesis that upper-asthenosphere flow near spreading axes, is by solid state, cataclastic flow, albeit at high temperatures. Because the flow of the silicate matrix is neither horizontal nor everywhere perpendicular to the spreading axes, a small diapiric focus is preferred. The pluton that fed the Troodos harzburgites would have been approximately 30 km in diameter, estimating from the angle of flow-foliation and discordance of AMS and AARM lineations. Of course, the regional scale of the mantle sequence would have required multiple, successive diapirs. Late in the cataclastic flow of the Troodos harzburgites, magnetite (re-)crystallized, accompanied and followed by the alteration of olivine to serpentine and iddingsite. Most of the magnetite occurs as separate grains, thus giving rise to an independent petrofabric element that documents a later, steep NW-upwards extension.

Acknowledgements

This work was funded by grants to Dr G.J. Borradaile from the Natural Sciences and Engineering Research Council of Canada (NSERC). It would not have been possible without the considerable logistical support and help of the Geological Survey Department of Cyprus, especially the Director, Dr George Petrides, as well as Dr Costas Xenophontos and Dr Ioannis Panayides. Sam Spivak and Anne Hammond are thanked for invaluable technical support.

References

Allerton, S., Vine, F.J., 1987. Spreading structure of the Troodos Ophiolite, Cyprus: some paleomagnetic constraints. Geology 15, 593–597.

Allerton, S., Vine, F.J., 1991. Spreading evolution of the Troodos Ophiolite, Cyprus. Geology 19, 637–640.

Borradaile, G.J., 1987. Anisotropy of magnetic susceptibility: rock composition versus strain. Tectonophysics 138, 327–329.

Borradaile, G.J., 1988. Magnetic susceptibility, petrofabrics and strain. Tectonophysics 156, 1–20.

Borradaile, G.J., 1991. Correlation of strain with anisotropy of magnetic susceptibility (AMS). Pure Appl. Geophys. 135, 15–29.

Borradaile, G.J., Henry, B., 1997. Tectonic applications of magnetic susceptibility and its anisotropy. Earth Sci. Rev. 42, 49–93.

Borradaile, G.J., Lagroix, F., 2000. Magnetic characterization of limestones using a new hysteresis projection. Geophys. J. Internat. 141, 213–226.

Borradaile, G.J., Stupavsky, M., 1995. Anisotropy of magnetic susceptibility: measurement schemes. Geophys. Res. Lett. 22, 1957–1960.

Borradaile, G.J., Werner, T., 1994. Magnetic anisotropy of some phyllosilicates. Tectonophysics 235, 233–248.

Borradaile, G.J., Keeler, W., Alford, C., Sarvas, P., 1987. Anisotropy of magnetic susceptibility of some metamorphic minerals. Phys. Earth Planet. Interiors 48, 161–166.

Borradaile, G.J., MacKenzie, A., Jensen, E., 1990. Silicate versus trace mineral susceptibility in metamorphic rocks. J. Geophys. Res. 95, 8447–8451.

Borradaile, G.J., Fralick, P.W., Lagroix, F., 1999. Acquisition o;f anhysteretic remanence and tensor subtraction from ARM isolates true paleocurrent grain alignments. In: Tarling, D.H., Turner, P. (Eds.). Palaeomagnetism and Diagenesis in Sedimemts. Geological Society, London, pp. 139–145 Spec. Publ. No. 151.

Carmichael, R.S., 1982. CRC Handbook of Physical Properties of Rocks and Minerals. CRC Press, Boca Raton, Florida (741pp.).

Clube, T.M.M., Robertson, A.H.F., 1986. The paleorotation of the Troodos microplate, Cyprus, in the Late Mesozoic–Early Cenozoic plate tectonic framework of the Eastern Mediterranean. Surv. Geophys. 8, 375–437.

Cueleneer, G., Nicolas, A., Boudier, F., 1988. Mantle flow patterns at an oceanic spreading centre: the Oman peridotites record. Tectonophysics 151, 1–26.

Day, R., Fuller, M.D., Schmidt, V.A., 1977. Hysteresis properties of

titanomagnetites: grain size and compositional dependence. Phys. Earth Planet. Interiors 13, 260–267.

Droop, G.T.R., 1987. A general equation for estimating Fe^{3+} concentrations in ferromagnesian silicates and oxides from microprobe analyses, using stoichiometric criteria. Min. Mag. 51, 431–435.

Dunlop, D.P., Özdemir, Ö., 1997. Rock Magnetism: Fundamentals and Frontiers. Cambridge University Press, Cambridge, MA (573pp.).

Gass, I.G., 1990. Ophiolites and oceanic lithosphere. In: Troodos '87, Ophiolite and Oceanic Lithosphere, Cyprus Geological Survey Department, pp. 1–10.

Gass, I.G., MacLeod, C.J., Murton, B.J., Panayiotou, A., Simonian, K.O., Xenophontos, C., 1994. The geology of the southern Troodos transform fault zone. Geological Survey Department, Nicosis, Cyprus Memoir no. 9, 218pp.

Henry, B., 1983. Interprétation quantitative de l'anisotropie de susceptibilité magnétique. Tectonophysics 91, 165–177.

Hrouda, F., 1982. Magnetic anisotropy of rocks and its application in geology and geophysics. Geophys. Surv. 5, 37–82.

Hrouda, F., 1993. Theoretical models of magnetic anisotropy to strain relationship revisited. Phys. Earth Planet. Interiors 77, 237–249.

Hrouda, F., Schulmann, K., 1990. Conversion of the magnetic susceptibility tensor into the orientation tensor in some rocks. Phys. Earth Planet. Interiors 63, 71–77.

Hrouda, F., Henry, B., Borradaile, G.J., 2000. Limitations of tensor subtraction in isolating diamagnetic fabrics by magnetic anisotropy. Tectonophysics 322, 303–310.

Jackson, M., 1991. Anisotropy of magnetic remanence: a brief review of mineralogical sources, physical origins, and geological applications and comparison with susceptibility anisotropy. Pure Appl. Geophys. 136, 1–28.

Jackson, M.J., Tauxe, L., 1991. Anisotropy of magnetic susceptibility and remanence: developments in the characterization of tectonic, sedimentary, and igneous fabric. Rev. Geophys. 29, 371–376 (suppl, IUGG Report Contributions in Geomagnetism and Paleomagnetism).

Jackson, M., Borradaile, G.J., Hudleston, P.J., Banerjee, S.K., 1993. Experimental deformation of synthetic magnetite-bearing calcite sandstones: effects on remanence, bulk magnetic properties, and magnetic anisotropy. J. Geophys. Res. 98, 383401.

Jelinek, V., 1981. Characterization of the magnetic fabric of rocks. Tectonophysics 79, 63–67.

King, J., Banerjee, S.K., Marvin, J., Özdemir, Ö., 1982. A comparison of different magnetic methods for determining the relative grain size of magnetite in natural materials: some results from lake sediments. Earth Planet. Sci. Lett. 59, 404–419.

Lagroix, F., Borradaile, G.J., 2001. Misinterpretation of magnetic fabrics due to crystallographic and impurity control in mafic silicates. Tectonophysics, 1 in press.

McCabe, C., Jackson, M., Ellwood, B., 1985. Magnetic anisotropy in the Trenton Limestone: results of a new technique, anisotropy of anhysteretic susceptibility. Geophys. Res. Lett. 12, 333–336.

Moores, E.M., Robinson, P.T., Malpas, J., Xenophontos, C., 1984. A model for the origin of the Troodos Massif, Cyprus and other mid-east ophiolites. Geology 12, 500–503.

Murton, B.J., 1990. Was the Southern Troodos Transform Fault a victim of microplate rotation? In: Troodos '87, Ophiolite and Oceanic Lithosphere, Cyprus Geological Survey Department, pp. 87–98.

Nicolas, A., Poirier, J.P., 1976. Crystalline Plasticity and Solid State Flow in Metamorphic Rocks. Wiley, New York (444pp.).

Poirier, J-P., 1985. Creep of Crystals: High-temperature Deformation Processes in Metals, Ceramics and Minerals. Cambridge University Press, New York (260pp.).

Richter, C., van der Pluijm, B.A., 1993. Separation of paramagnetic and ferrimagnetic susceptibilities using low temperature magnetic susceptibilities and comparison with high field methods. Phys. Earth Planet. Interiors 82, 113–123.

Robertson, A.H.F., 1990. Tectonic evolution of Cyprus. In: Troodos '87, Ophiolites and Oceanic Lithosphere, Cyprus Geological Survey Department, pp. 235–250.

Robinson, P.T., Malpas, J., 1987. The Troodos ophiolite of Cyprus: new perspective on its origin and emplacement. In: Troodos '87, Ophiolites and Oceanic Lithosphere, Cyprus Geological Survey Department, pp. 13–26.

Rochette, P., 1987. Magnetic susceptibility of the rock matrix related to magnetic fabric studies. J. Struct. Geol. 9, 1015–1020.

Rochette, P., 1988. Mathematical model relationship between the paramagnetic anisotropy and strain in slates—discussion. Tectonophysics 156, 313–315.

Rochette, P., 1994. Comments on "Anisotropic magnetic susceptibility in the continental lower crust and its implications for the shape of magnetic anomalies" by G. Florio et al.. Geophys. Res. Lett. 21, 2773–2774.

Rochette, P., Fillion, G., 1988. Identification of multicomponent anisotropies in rocks using various field and temperature values in a cryogenic magnetometer. Phys. Earth Planet. Interiors 51, 379–386.

Rochette, P., Jackson, J., Aubourg, C., 1992. Rock magnetism and the interpretation of anisotropy of magnetic susceptibility. Rev. Geophys. 30, 209226.

Syono, Y., 1960. Magnetic susceptibility of some rock forming silicate minerals such as amphiboles, biotites, cordierites and garnets. J. Geomagnet. Geoelectricity 11, 85–93.

Tarling, D.H., Hrouda, F., 1993. The Magnetic Anisotropy of Rocks. Chapman and Hall, London (217pp.).

Wasilewski, P.J., 1973. Magnetic hysteresis in natural materials. Earth Planet. Sci. Lett. 20, 67–72.

Werner, T., Borradaile, G.J., 1996. Paleoremanence dispersal across a transpressional Archean terrain: Deflection by anisotropy or by late compression? J. Geophys. Res. 101, 5531–5545.